Gravity Data Decomposition Based on Spectral Analysis and Halo Wavelet Transform, Case Study at Bird's Head Peninsula, West Papua

Accep Handyarso[1,*] & Wawan Gunawan A. Kadir[2]

[1]Geophysics Group, Centre of Geological Survey, Indonesia Geological Agency, Building B 1st Floor, Jalan Diponegoro 57, Bandung 40122, Indonesia.
[2]Faculty of Mining and Petroleum Engineering, Institut Teknologi Bandung, Basic Science Center B 2nd Floor, Jalan Ganesha 10, Bandung 40132, Indonesia.
*E-mail: accep.handyarso@esdm.go.id

Abstract. Gravity imagery is commonly used in the preliminary study of sedimentary basins. Gravity data have an excellent lateral resolution but poor vertical resolution. The gravity response represents the superposition of all elements of differing density contrasts and depths for a given region below the surface. The ability to perform depth-based gravity data decomposition is important for the interpretation of the data. This can be achieved by combining spectral analysis with the Halo wavelet transform. The decomposition method was tested using synthetic data as well as field data collected at Bird's Head Peninsula, West Papua. Examination of the proposed method using the synthetic data produced satisfactory results that corresponded well to the models. The test using the field data clearly imaged anticline structures that formed due to the ongoing collision of the Australia Continental Plate and the Pacific Oceanic Plate. In part of the Lengguru Fold and Thrust Belt, the folding structures are not imaged at depths greater than ~6 km. We propose that folding structures are not found at deeper levels. The gravity imagery also indicates that the Sorong Fault Zone breaks apart into several segments, which causes other perpendicular lineaments (strike-slip faulting). These strike-slip faults are clearly visible in the Bird's Head Region.

Keywords: *gravity; Halo wavelet; spectral analysis; Indonesia; Papua New Guinea.*

1 Introduction

Gravity data are commonly used to image the subsurface density contrast distribution for a given area [1]. Gravity data have an excellent lateral resolution but a poor vertical resolution. This is because the gravity response represents the superposition of all elements (from top to bottom) and these elements may have different densities. Therefore, gravity data separation is a must before proceeding to data interpretation. Typically, the decomposition process is used to determine the gravity response from shallow source anomalies or deep source anomalies.

Received December 9th, 2016, 1st Revision May 4th, 2017, 2nd Revision July 20th, 2017, Accepted for publication September 4th, 2017.
 ISSN: 2337-5779, DOI: 10.5614/j.eng.technol.sci.2017.49.4.1

There are various decomposition processes that can be applied to gravity data. These include the graphical method, upward continuation, polynomial surface fitting and trend surface analysis (TSA), windowed moving average, spectral analysis, linear and non-linear filtering. The decomposition process using the graphical method is also known as hand smoothing. This is done manually, so it is not recommended for large or high-resolution data sets. The upward continuation method is also commonly used [1]. However, this method has two disadvantages. Short-wavelength and long-wavelength data are both attenuated because of the implication of continuation. The upward continuation method also requires elevation information to be known before processing [2]. Trend surface analysis and polynomial surface fitting are surface regression based methods. These methods are generally performed using bilinear equations or second-order polynomial equations. The difference between the TSA result and the Bouguer anomaly is called the residual anomaly.

In the last decade, the use of wavelet transforms in the decomposition process of gravity data has become increasingly popular. The multi-scale analysis capabilities inherent in the wavelet transform method increase its flexibility during implementation. Digital wavelet transforms (DWT) can be used for regional-residual data separation in gravity data [3]. The application of wavelet transforms also gives satisfactory results when applied to magnetic data [4]. The decomposition process of gravity data in China using DWT gave feasible results according to observed geology and field data [5]. In addition, the wavelet transform can also be used for various other purposes, such as removing noise from gravity data [6], finding the boundaries of anomaly sources [7], and for gravity data inversion [8].

The decomposition method proposed in this paper was developed based on an integration between Halo wavelet transform and spectral analysis. The proposed method was tested using a synthetic data set as well as a field data set. The spectral analysis technique is involved in the proposed method because it provides an average depth estimation of the particular features identified from the gravity imagery. Using this average depth, the correct wavenumber associated with the targeted depth can be defined and this wavenumber is then used by the Halo wavelet transform during the decomposition process. The common regional-residual decomposition process only provides the output of the residual anomaly contour and the regional anomaly contour. In this paper, synthetic data were designed such that there are middle anomaly sources. The proposed decomposition method is expected to be able to separate each anomaly source according to the depth-based decomposition of the gravity data.

The field data were collected at Bird's Head Peninsula, West Papua. This area was selected because of its recorded complex pattern of geological structures.

The applied decomposition method was expected to be able to delineate the presence of subsurface geological structures and to estimate its depth.

2 Methods

2.1 Spectral Analysis

Spectral analysis is performed to decompose anomaly signals based on the wavelength so the average depth of the anomaly sources can be estimated. The average depth of the anomaly sources can be calculated based on the slope of the spectral diagram (wavelength versus power spectral magnitude). The depth in anomaly source estimation for the gravity data can be expressed as follows [2]:

$$Depth = \frac{P(r_2)-P(r_1)}{4\pi(r_2-r_1)} \tag{1}$$

Eq. (1) is essentially a straight line gradient calculation of the power spectral $P(r)$ value in the logarithmic form of the FFT magnitude result, while r is the corresponding wavelength. The result of the calculation using Eq. (1) generates a relation in which power spectral density is a function of depth and can be defined as an exponential equation according to depth h [9,10,11] in Eq. (2) as follows:

$$P = se^{-2kh} \tag{2}$$

where s is a constant proportional to the equivalent layer and k is the angular vector.

2.2 Halo Wavelet

The wavelet transform was first introduced in 1980 by Morlet, a French research scientist working on seismic data analysis [12]. A Morlet wavelet has both magnitude and direction [13]. The vector $t = (t_1, t_2)$ is defined on the two-dimensional plane with a magnitude equation expressed in Eq. (3) as follows:

$$|t| = \sqrt{t_1^2 + t_2^2} \tag{3}$$

The two-dimensional Morlet wavelet, both in the spatial domain and in the frequency domain, is then given in Eq. (4) and Eq. (5) as follows:

$$\omega^{\theta}(t) = \frac{1}{\sqrt{\pi}} e^{-i\Omega^0 t} e^{|t|^2/2} \text{ for } \Omega^0 \geq 5 \tag{4}$$

$$\widehat{\omega}^{\theta}(\Omega) = \frac{1}{\sqrt{\pi}} e^{-|\Omega-\Omega^0|^2/2} \tag{5}$$

where $\Omega = (\omega_1, \omega_2)$ is an arbitrary point on a two-dimensional frequency plane and $\Omega^0 = (\omega_1^0, \omega_2^0)$ is a constant. The superscript θ indicates the direction of the wavelet and can be expressed in Eq. (6) as follows:

$$\theta = tan^{-1}\left(\frac{\omega_2^0}{\omega_1^0}\right) \tag{6}$$

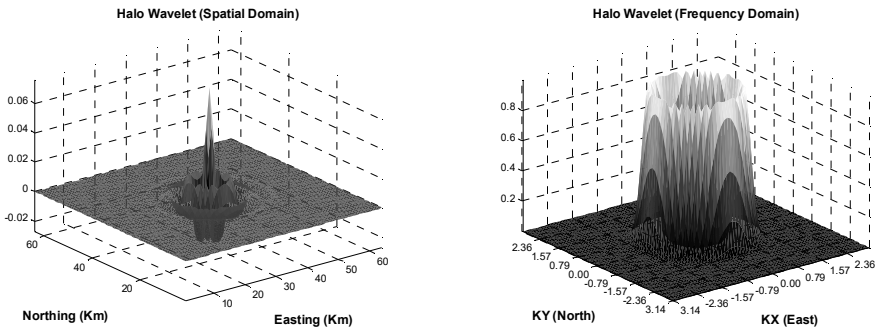

(a) (b)

Figure 1 Halo wavelet visualization in the spatial domain (a) and in the frequency domain (b).

The Halo wavelet is a modification of the Morlet wavelet that ignores the Morlet wavelet directional factor. The result of this Morlet wavelet modification is called a Halo wavelet because of its shape in the frequency domain [14]. In the frequency domain, the Halo wavelet is defined using Eq. (7):

$$\psi(\Omega) = ne^{\frac{-(|\Omega|-|\Omega^0|)^2}{2}} \tag{7}$$

where n is a normalization factor. Visualizations of the Halo wavelet in both the spatial and the frequency domain are shown in Figures 1a and 1b respectively.

2.3 Algorithm

The algorithm of the proposed decomposition method may be implemented in two alternative ways. The first is to use the method in the spatial domain, which is a convolution process, and the second is to use it in the frequency domain, which is a more simple multiplication process. In this paper, the calculation was performed in the frequency domain. The Fourier domain representation of the proposed method can be expressed as follows:

$$\mathcal{F}\left(g_z^b\right) = \mathcal{F}(g_z) \cdot \mathcal{F}\left(\psi^b\right) \tag{8}$$

$$g_z^b = \mathcal{F}^{-1}\left[\mathcal{F}(g_z) \cdot ne^{\frac{-(|\Omega|-|\Omega^0|)^2}{2}}\right] \tag{9}$$

where $\mathcal{F}\left(g_z^b\right)$ is the Fourier transform of the bandpass-filtered gravity measurement result g_z on the surface, $\mathcal{F}(g_z)$ is the two-dimensional Fourier transform of g_z, and $\mathcal{F}\left(\psi^b\right)$ is the Halo wavelet transform in the frequency domain, which is equal to Eq. (7). Substituting Eq. (7) into Eq. (8) gives Eq. (9), where g_z^b are the bandpass-filtered gravity data in the spatial domain, i.e. the output data of the proposed method. Calculation of Eq. (9) requires a constant value of Ω^0, which behaves as a center frequency (f_c) of the Halo wavelet, in this case it is a certain constant wavenumber associated with the targeted depth. Parameter Ω^0 can be acquired through piecewise linearization of the wavenumber-power spectral function from Eq. (1) and a curve fitting algorithm was utilized to reverse it back to get the depth-wavenumber function such that every depth value will be associated with a certain wavenumber.

3 Result and Analysis

3.1 Synthetics Data

The proposed gravity data decomposition method was tested using synthetic data and field data. In the case of the synthetic data, the subsurface model consisted of ten cubes grouped into three colors, i.e. red, green, and blue cubes (Figure 2). The red cubes represent the deepest areas and these act as regional anomaly sources. The green and blue cubes are located at shallower depths and represent residual anomaly sources. The gravity response model is a superposition of all cubes below the surface.

The forward modeling calculation uses a formula of the gravity response from rectangular bodies [15]. The model area was 50 x 50 km^2. The forward modeling scheme calculates the gravity response on the surface from each colored group of cubes. Forward modeling thus obtains three kinds of anomaly contours, i.e. an upper residual anomaly contour, a lower residual anomaly contour, and a regional anomaly contour (Figure 3). The synthetic Bouguer anomaly data are a superposition of these three anomaly contours. The 3D subsurface model parameters used in this paper are summarized in Table 1.

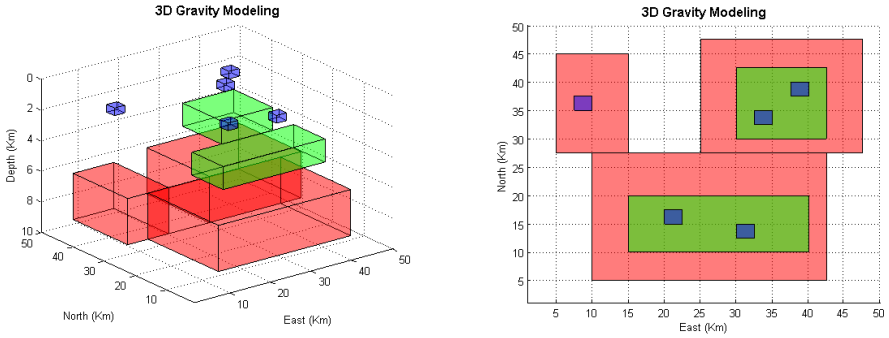

(a) (b)

Figure 2 Subsurface of the 3D cuboid model: perspective view (a), and top view (b). The model consists of 10 cubes, categorized based on color.

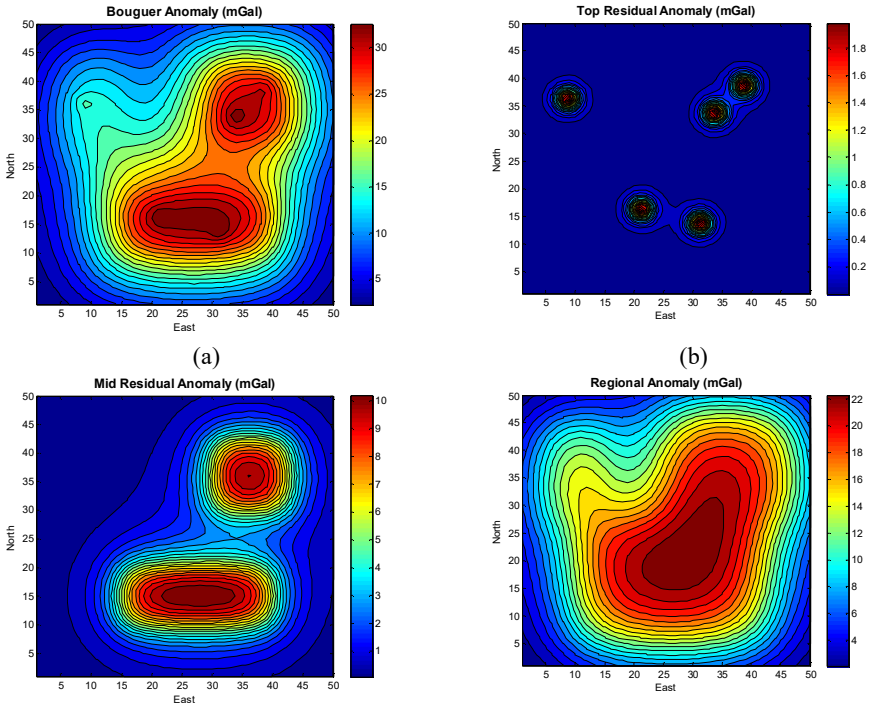

(a) (b)

(c) (d)

Figure 3 Gravity contour from forward modeling result at mGal scale, consistsing of: complete Bouguer anomaly (a), upper residual anomaly (b), lower residual anomaly (c), and regional anomaly (d).

Spectral analysis of the synthetic data showed that the energy is concentrated in the lower wavenumber, especially in the 0~0.4 rad/km band. This band is a

regional anomaly. A residual anomaly is located in the 0.4~1.8 rad/km band. Spectrum energy above 1.8 rad/km is classified as noise in the data. On the residual band, i.e. at 0.4~1.8 rad/km, there are two residual anomalies mixed in the spectrum.

Table 1 Summary of physical parameters of 3D Cuboid subsurface model.

Parameters		A1	A2	A3	B1	B2	C1	C2	C3	C4	C5
Dimension	L	32.5	22.5	10	25	12.5	2.5	2.5	2.5	2.5	2.5
(km)	W	22.5	20	17.5	10	12.5	2.5	2.5	2.5	2.5	2.5
	T	3	3	3	1.5	1.5	0.5	0.5	0.5	0.5	0.5
Mass	X	26.25	36.25	10	27.5	36.25	21.25	31.25	33.75	38.75	8.75
Centre	Y	16.25	37.5	36.25	15	36.25	16.25	13.75	33.75	38.75	36.25
(km)	Z	7.5	7.5	7.5	3.75	3.75	1.25	1.25	1.25	1.25	1.25
Rho (kg/m3)		300	300	300	300	300	300	300	300	300	300

The decomposition result of the filtering technique consists of three patterns of anomalies, i.e. an upper residual anomaly contour, a lower residual anomaly contour, and a regional anomaly contour, as shown in Figure 4. The filtering parameters used during decomposition were ZDEPTH = 7.5 km for the regional anomaly target, ZDEPTH = 3.5 km for the lower residual anomaly target, and ZDEPTH = 0.5 km for the upper residual anomaly target. The ZDEPTH parameter will be used to calculate the corresponding wavenumber according to an exponential scaling factor.

The deeper anomaly pattern can still be observed in the filtered decomposition result from the synthetic data. This is because the gravity response on the surface is a superposition of all the elements below the surface and its overlap between the deeper anomaly sources and the shallower anomaly sources. Hence, the decomposition result in the gravity data anomalies cannot be done perfectly [16]. This is a natural characteristic of the gravity method. The wavenumber spectrum of most features are broadband, so the spectrum of features at different depths will always overlap and, consequently, the features cannot be separated completely using a wavelet filtering technique (or by using other methods). However, it is possible to predict the value of a given gravity anomaly at a certain depth. Using this predicted value, the anomaly sources under the surface at a certain depth can be estimated. In this way, the vertical resolution problems of the gravity method can be reduced.

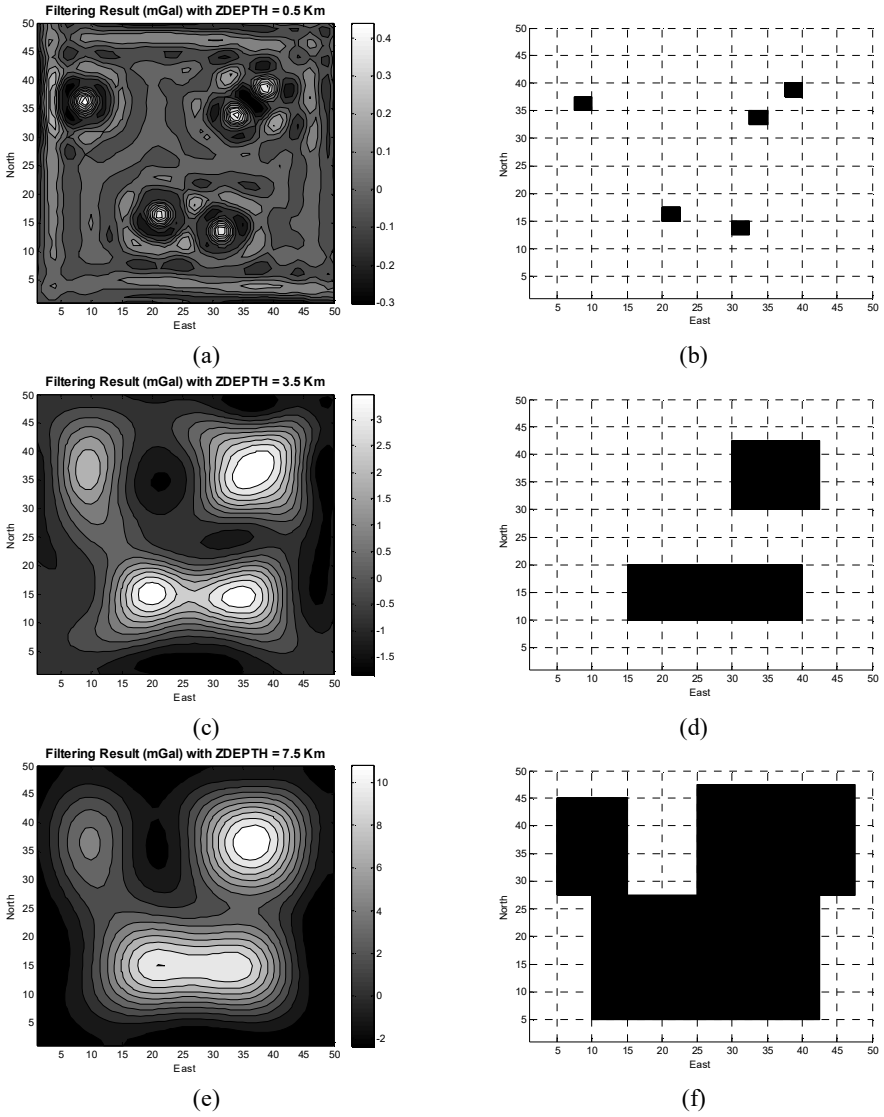

Figure 4 Decomposition result using synthetics data based on the Halo wavelet transform. It provides an upper residual anomaly (a) with the same lateral pattern as the upper cuboid model (b), a lower residual anomaly (c) with the same lateral position as the middle cuboid model (d), and a regional anomaly (e) with the same position as the lower cuboid model (f).

The decomposition result based on the Halo wavelet transform and spectral analysis shows its capability to separate the anomaly sources according to the depth of the target sources. The results show that the anomaly sources can be

located laterally at certain depths and close to the designed subsurface model, so the proposed method can be used to handle the field data for further processing.

3.2 Field Data Applications

The field data set in this paper were compiled from several resources. The basic data were taken from a publicly available free-air gravity data set from TOPEX [17] as well as TOPEX's topographic data set. The free-air gravity data set used in this paper was converted to its Bouguer gravity anomaly using the FA2BOUG software application [18]. After calculating the Bouguer anomaly data set from the free-air gravity data set, the public gravity data were leveled to the Indonesia Geological Research and Development Centre (GRDC) gravity database. This approximation was applied to improve the coarse resolution (~5-10 km) of the GRDC gravity database. Our overall aim was to make the best fit (surface fitting) of the global publicly available gravity data set (TOPEX data set) to the GRDC gravity database, which consists of data points that were measured directly on the ground. This method resulted in almost the same values between the GRDC data set and the TOPEX data set, which represents a more comprehensive spatial coverage. This means that the leveled TOPEX Bouguer data should produce a more detailed representation of the subsurface geology and improve the data resolution of the original GRDC data set.

The gravity and topographic data sets have a spatial resolution of 1 x 1 arc minutes grid (~1.67-2 km). This public gravity data set resolution is qualified for study purposes within regions. In addition, the data set was leveled to ground gravity data measured directly on the Earth's surface. This is the simplest, cheapest and fastest method, as opposed to collecting measurements across the whole region as part of a field campaign (which would be impossible considering the terrain and dense vegetation) or via airplane (which would require huge funding). If there is an interesting area, then detailed measurements should be performed. The Bouguer anomaly map used in this paper is shown in Figure 5. The Bintuni Basin, Salawati Basin and other basins (e.g. Cendrawasih Bay, Nothern Seram Island) are clearly visible as low gravity anomalies (indicated by dark colors).

The Halo wavelet transform and spectral analysis as the proposed gravity data decomposition method were implemented at several depth intervals in the field data set. The result of the application of the gravity data decomposition method to the field data is shown in Figures 6, 7 and 8. The decomposition method was first implemented for filtering out the Bouger anomalies (Figure 5) at each depth layer, then the second vertical derivative (SVD) grid was calculated directly for each depth layer. The decomposition result for ZDEPTH = 2 km is

shown in Figure 6, ZDEPTH = 4 km result is shown in Figure 7, and ZDEPTH = 6 km result is shown in Figure 8.

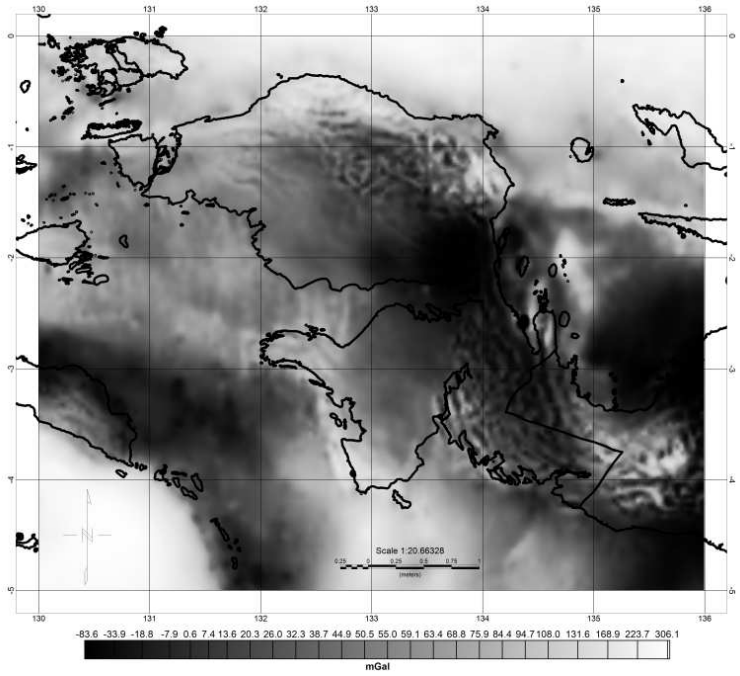

Figure 5 Bouguer anomaly map of Bird's Head Peninsula based on a global gravity dataset (TOPEX) after being leveled to the GRDC gravity data set. Low anomalies show up as dark areas while high anomalies are light.

There are several huge fault structures around Bird's Head Peninsula that are surrounded by lineaments. The Tarera-Aiduna Fault Zone (TAFZ) was not observed in this dataset. However, the Sorong Fault Zone (SFZ), Yapen Fault Zone (YFZ), Lengguru Fold and Thrust Belt and Onin-Kumawa Ridge can be identified in each grid (Figures 6-8). The lineaments imaged from the regional gravity data consist of faults and folds that are difficult to distinguish from one another. Comparing Figure 6 with the existing structural interpretations in Bird's Head Peninsula can be used to infer more about the nature of these large structures (i.e. determining if they are a fault or a fold). The light-colored (red-purple in Figure 7-8) lineaments are interpreted to represent highly folded structures or uplifted blocks (thrust on top of other crusts), while the grey (yellow-red in Figure 7-8) lineament areas represent regions that are covered by thick sediments (i.e. basins).

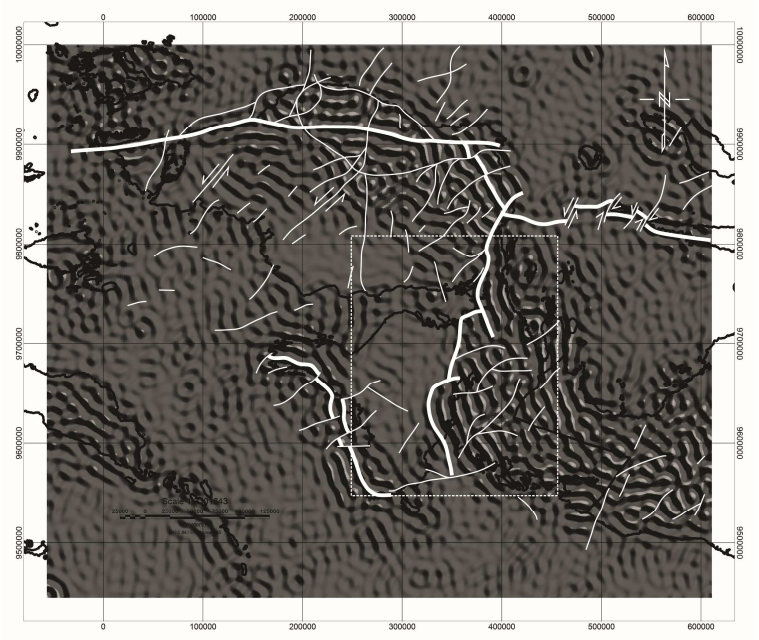

Figure 6 Second vertical derivative (SVD) from the decomposition result of the Bouguer anomaly (Figure 5) in Birds Head Peninsula of West Papua with ZDEPTH parameter at 2 km. Structural lineaments across the region at a depth of ~2 km are visible.

In general, it can be seen that there are many folding structures in Bird's Head Peninsula that formed due to the ongoing collision of Australia Continental Plate and Pacific Oceanic Plate. The folding structures at the Lengguru Fold and Thrust Belt tend to diminish at the deeper layers and completely disappear at 6 km depth (Figure 8). This situation can be seen through evaluation of Figures 6, 7 and 8 inside the square area. Hence, we propose that the folding structures in the Lengguru Fold and Thrust Belt are not continuous downward more than 6 km. In other words, there are possibly sediment layers under the folding structures that may have hydrocarbon potential. This result is comparable with the geological section of the Lengguru Fold and Thrust Belt in the geological map of the Kaimana sheet [19]. According to the Geological map of the Kaimana sheet, part of the Bintuni Basin is spread out below the folding structures of the Lengguru Fold and Thrust Belt at depths of ~4-5 km. The Bintuni Basin separates the Onin-Kumawa Ridge from the Lengguru Fold and Thrust Belt structures in Bird's Head Peninsula region.

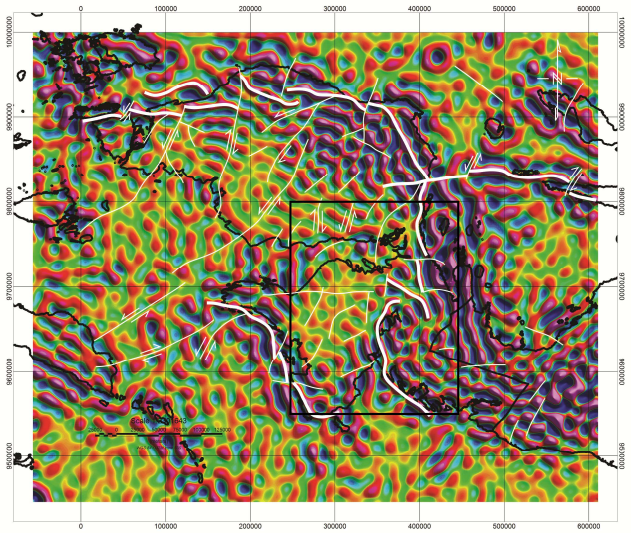

Figure 7 SVD from the decomposition result with ZDEPTH parameter at 4 km. It shows that the main structures around the Lengguru Fold and Thrust Belt and the Sorong Fault Zone are breaking up into several segments below the surface. All faults consist of small segments that are interlinked. There are more segments compared to nearer to the surface.

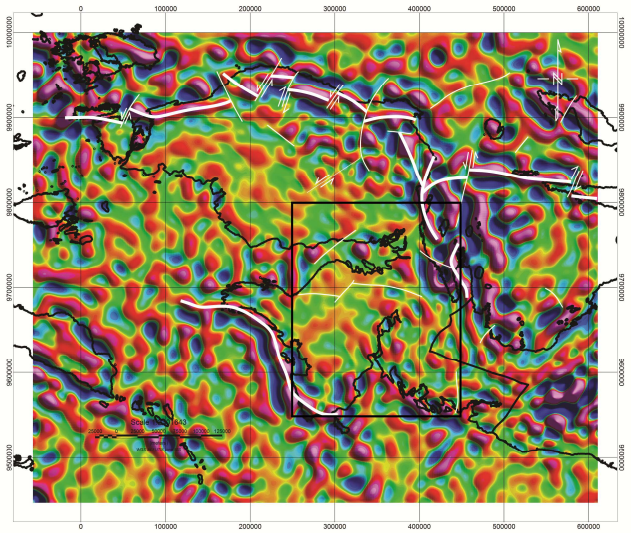

Figure 8 SVD from the decomposition result with ZDEPTH parameter at 6 km. It shows that the Sorong Fault Zone breaks up into several segments under the surface while the Lengguru Fold and Thrust Belt disappear at ~6 km depth.

If we put more attention to the Sorong Fault Zone (SFZ), the SFZ is relatively continuous at 2 km depth, but these structures seem to be fragmented at deeper positions, such as 4 km and 6 km depth (e.g. Figures 6-8). There are many segments with random lineaments along the SFZ, as can be seen in Figures 7 and 8. In contrast with the Onin-Kumawa Ridge these areas have continuous structures at 6 km depth, although it is segmented at shallower depth, as shown in Figures 6-8.

The relative motion between the Pacific Oceanic Plate and the Australian Continental Plate will cause perpendicular strike-slip fault movement along the SFZ. In Bird's Head Peninsula this has occurred due to compressional forces in the opposite direction, causing translation and rotation simultaneously [20]. The resistance of the Sorong Fault Zone (SFZ) surface and the Yapen Fault Zone (YFZ) surface is not uniform in every place, there are some areas that are weaker than others. The movement speed of the Pacific Plate relative to the Australia Plate, which is not the same along the SFZ and YFZ, causes the SFZ and the YFZ to break apart into several segments, as can be seen from Figures 7 and 8. When the SFZ breaks into several segments, it will be followed by strike-slip fault movement relatively perpendicular to the SFZ trend direction. These phenomena are also found along the YFZ [21]. The SFZ lineaments and its perpendicular strike-slip fault lineaments fulfill Anderson's theory of faulting, which is indicated by the X-shaped conjugate fault pattern structures with an intersection angle of ~30 degrees between the maximum compressive stress and the fault. The SFZ breaks up into several segments below the surface. All faults consist of small segments that are interlinked.

Implementation of the proposed decomposition method to the gravity data shows that the Lengguru Fold and Thrust Belt were not imaged at deeper levels (~6km) while the Sorong Fault Zone breaks apart into several segments at around ~4-6 km beneath the surface. The breakoff of the SFZ is followed by strike-slip fault relatively perpendicular to SFZ and these new structure patterns are clearly visible from the gravity imagery. Further research is needed to compare this result with other geophysical method results (e.g. seismic reflection), particularly in sedimentary basins.

4 Conclusions

The decomposition method proposed in this paper provided an accurate representation of the synthetic data. The anomaly sources could be localized correctly according to the corresponding depth. In addition to field data application, we found that the folding structures at the Lengguru Fold and Thrust Belt (LFTB) were not imaged at depths greater than ~6 km. This could be due to the sediment layer in the Bintuni Basin that is spread out under the

folding structures. In the Sorong Fault Zone (SFZ) area, it was found that the SFZ breaks apart into several segments beneath the surface. However, the subsurface structures underneath the Onin-Kumawa Ridge behave differently. The processed gravity imagery clearly shows the orientation of the structural lineaments. For instance, there are lineaments of the SFZ and its strike-slip fault as a conjugate pattern that trends almost perpendicular to the SFZ. We propose that the 'cross-structures' occurred because of the ongoing collision between the Australian (continental) plate and the Pacific (oceanic) plate. While these are hypothetical conclusions, we suggest it is reasonable to explain the gravity data contours obtained from the wavelet decomposition result. The ability of the proposed decomposition method to look below the Lengguru Fold and Thrust Belt provides a way for researchers to explore under cover and to deal with difficult geological environments such as basins with volcanic rocks or thick limestone sequences that cannot be easily imaged with other geophysical techniques (e.g. seismic). Furthermore, the proposed method may be utilized and developed further to delineate Cenozoic and Pre-Cenozoic basin separations.

Acknowledgements

The authors are most grateful for the support of the Centre of Geological Survey-Indonesia Geological Agency (previously called GRDC). We also sincerely thank the reviewers for their valuable suggestions.

References

[1] White, L.T., Morse, M.P. & Lister, G.S., *Lithospheric-Scale Structures in New Guinea and Their Control on The Location of Gold and Copper Deposits*, Solid Earth 5, **5**(1), pp. 163-179 (doi:10.5194/se-5-163-2014), 2014.

[2] Ghuo, L., Meng, X., Chen, Z., Li, S. & Zheng, Y., *Preferential Filtering for Gravity Anomaly Separation*, Computer & Geosciences, **51**, pp. 247-254, 2013.

[3] Fedi, M. & Quarta, T., *Wavelet Analysis for the Regional-Residual and Local Separation of the Potential Field Anomalies*, Geophys Prospect, **46**(5), pp. 507-525, 1998.

[4] Ucan, O.N., Seker, S., Albora, A.M. & Ozmen, A., *Separation of Magnetic Field in Geophysical Studies Using a 2-D Multi-Resolution Wavelet Analysis Approach*, J. Balkan Geophysics Soc., **3**(3), pp. 53-58, 2000.

[5] Yang, W.C., Shi,Z.Q. & Hou, Z.Z., *Discrete Wavelet Transform for Multiple Decomposition of Gravity Anomalies*, Chin. J. Geophys, **44**(4), pp. 529-537, 2001.

[6] Lyrio, J.C.S., Tenorio, L. & Li, Y., *Efficient Automatic Denoising of Gravity Gradiometry Data*, Geophysics, **69**(3), pp. 772-782, 2004.
[7] Martelet, G., Sailhac, P., Moreau, F. & Diament, M., *Characterization of Geological Boundaries Using 1-D Wavelet Transform on Gravity Data: Theory and Application to the Himalayas*, Geophysics, **66**(4), pp. 1116-1129, 2001.
[8] Saihac P. & Gilbert D., *Identification of Sources of Potential Fields with the Continous Wavelet Transform: Two-Dimensional Wavelet and Multipolar Approximations*, J. Geophys. Res., **108**(B5), pp. 2262, 2003.
[9] Naidu, P., *Spectrum of the Potential Field Due to Randomly Distributed Sources*, Geophysics, **33**(2), pp. 337-345, 1968.
[10] Dampney, C.N.G., *The Equivalent Source Technique*, Geophysics, **34**(1), pp. 39-53, 1969.
[11] Xu, Y., Hao, T., Li, Z., Duan, Q. & Zhang, L., *Regional Gravity Anomaly Separation Using Wavelet Transform and Spectrum Analysis*, Journal of Geophysics and Engineering, **6**(3), 2009.
[12] Koornwinder, T.H., *Wavelet: An Elementary Treatment of Theory and Applications*, pp. 1-12, World Scientific Publishing Co. Inc., 1993.
[13] Kumar, Praveen & Foufoula-Georgiou, Efi, *Wavelet Analysis in Geophysics: An Introduction*, Academic Press California, United States of America, 1994.
[14] Dallard, T. & Spedding, G.R., *2D Wavelet Transform*, Preprint, 1990.
[15] Blakely, R.J., *Potential Theory in Gravity and Magnetic Application*, Cambridge University Press, 1995.
[16] Telford, W.M., Geldart, L.P. & Sheriff, R.E., *Applied Geophysics,* 2nd Edition, Cambridge University Press, Cambridge, 2004.
[17] Extract XYZ Grid – Topography or Gravity, http://topex.ucsd.edu/cgi-bin/get_data.cgi.
[18] Fullea, J., Fernandez, M. & Zeyen, H., *FA2BOUG – a FORTRAN 90 Code to Compute Bouguer Gravity Anomalies from Gridded Free-Air Anomalies: Application to the Atlantic Mediterranean Transition Zone*, Comput. Geosci., **34**(12), pp. 1665-1681, 2008.
[19] Tobing, S.L., Robinson, G.P. & Ryburn, R.J., *Geological Map of the Kaimana Sheet Scale 1:250.000*, Irian Jaya, GRDC, Bandung, 1990.
[20] Sapiie, B., Naryanto, W., Adyagharini, A.C. & Pamumpuni, A., *Geology and Tectonic Evolution of Bird Head Region Papua, Indonesia: Implication for Hydrocarbon Exploration in Eastern Indonesia*, Search & Discovery Article, No. 30260, 2012.
[21] Ikhwanudin, F. & Abdullah, CI., *Indication Strike Slip Movement a Part of Sorong Fault Zone in Yapen Island, Papua*, Indonesia, GSTF Journal of Geological Sciences (JGS), **2**(1), pp. 25-33, 2015.